PERGAMON

International Journal of Solids and Structures 38 (2001) 9253–9265

INTERNATIONAL JOURNAL OF SOLIDS and STRUCTURES

www.elsevier.com/locate/ijsolstr

Buckling and postbuckling characteristics of the superelastic SMA columns

Muhammad Ashiqur Rahman, Jinhao Qiu *, Junji Tani

Institute of Fluid Science, Tohoku University, Katahira 2-1-1, Aoba-ku, Sendai-shi 980-8577, Japan

Received 4 August 2000

Abstract

Some unique buckling and postbuckling behaviors of the superelastic shape memory alloy (SMA) columns are observed for a wide range of slenderness ratio (L/k) and compared with those of the SUS304 and Al columns. The experimental method comprises of compressive loading on the columns much beyond the point of instability followed by unloading allowing them to recover the shapes. It is found from the load–deformation curves that among the three materials, the buckling load of the SMA column increases most significantly with the decreasing L/k and ultimately exceeds that of SUS304 column. Interestingly, during compression the SMA column with $L/k = 38$ exhibits two distinct peak loads, the second one being the higher, contrary to the trend that load falls off monotonously for other columns in the postbuckling region. Similarly, for $L/k = 28$ the SMA column can sustain significantly high load after a distinct change in the mode of deformation. Furthermore, for certain values of L/k, the recovery forces increase remarkably as the buckled SMA columns are gradually unloaded. If not too short, they can significantly recover the initial shapes when completely unloaded. The above phenomena can be attributed to the special nature of SMA's stress–strain curve and the superelasticity itself. On the other hand, for too high slenderness ratios, Al columns have slightly higher buckling loads compared to the SMA columns. However, both of the Al and SUS304 columns show large residual strains after the complete cycle.

Keywords: Loading–unloading cycle; Load–deformation curves; Postbuckling behaviors; Martensitic phase transformation; Recovery force

1. Introduction

The superelastic shape memory alloys (SMAs) have the unique capability to fully regain the original shape from a deformed state when the mechanical load, which causes the deformation, is withdrawn. For some superelastic SMA materials, the recoverable strains can be on the order of 10% (Brinson, 1993; Tobushi et al., 2000). This phenomenon, termed as the pseudoelasticity or, superelasticity (SE) is dependent on the stress-induced martensitic transformation (SIMT), which in turn depends on the states of temperature and stress of the SMA. SIMT is said to be a solid–solid, diffusionless, isothermal phase transformation from

* Corresponding author. Fax: +81-22-217-5264.
E-mail address: qiu@ifs.tohoku.ac.jp (J. Qiu).

0020-7683/01/$ - see front matter
PII: S0020-7683(01)00160-3

Nomenclature

A_f	Austenite finish temperature of the SMA material
δ, Δ	displacement of the moving fixture, δ/L
ε	residual axial strain of the columns after a complete cycle
I, k	least moment of inertia of the cross-sectional area, least radius of gyration
L	unsupported length of the columns at $P = 0$
P	axial compressive load
T	test temperature

a crystallographically more ordered parent phase (austenite) to a crystallographically less ordered product phase (martensite) (Auricchio and Sacco, 1997; Otsuka and Wayman, 1998). At a temperature higher than its characteristic temperature (A_f), SMA exists in the parent austenite phase. Thus, during loading SIMT typically starts in the SMA material at the critical stress and when the SIMT is over, the SMA is in the stress-induced martensite (SIM) phase. During unloading, again at a critical stress the reverse phase transformation starts (from the SIM to parent phase) and when it is complete the SMA returns to its parent austenite phase. The complete loading–unloading cycle shows a typical hysteresis loop and if the strain during loading is fully recoverable it becomes a closed one (Brinson, 1993).

Having the unique feature of SE (usually at room temperature) SMAs are used in various applications, from orthodontic wires to self-expanding micro-structures used in the treatment of hollow-organ or duct-system occlusions (Auricchio and Sacco, 1997; Otsuka and Wayman, 1998). Since SMAs display superelastic hysteresis behavior over large strain ranges, a significant amount of energy dissipation is possible. Thus superelastic SMAs can be suitably used in the structures as dampers (Gandhi et al., 1998; Liang and Rogers, 1997). Apart from these applications of the superelastic SMA, extensive studies are also reported mostly on the theoretical constitutive modeling for the same material (Kamita and Matsuzaki, 1998).

So far, the study on the buckling and postbuckling behaviors of common structures like columns made of the superelastic SMA materials has not been reported in the literature. Usually, too large deformation takes place immediately after a column buckles. Because of SE a buckled column can regain its shape when the load is withdrawn and can remain in its place of application to serve its purpose for repeated loading–unloading cycles. Observing the above fact, the present study extensively (for slenderness ratio 28–368) deals with the buckling and postbuckling behaviors of the superelastic SMA columns (some times termed only as the SMA columns) through a complete loading–unloading cycle. Similar experimental data are also obtained for SUS304 and Al columns under the same testing conditions for valid comparison.

Columns usually fail due to mechanical instability under external compressive loading. Predictions of buckling loads for structures solely based on eigenvalue solutions usually result in ideal and therefore much higher buckling loads than their real values during applications. Thus, according to Thompson and Hunt (1973), predictions of buckling loads for structures based on large deformation theory may yield more realistic solutions than the corresponding eigenvalue solutions under certain conditions as delineated below.

The buckling characteristics of any structure, whatever the type of buckling is, may be best comprehended if the equilibrium path of the deformed structure under load is determined for both the prebuckling and postbuckling zones. The first instability of the equilibrium equations on the primary equilibrium configuration path would correspond to the critical load for any type of buckling.

However, it is a well-known fact that, whatever may be the method of prediction, the theoretical buckling loads of structures are higher than those are during applications. The reasons behind this discrepancy

between the theoretical and practical buckling loads are mainly attributed to the unavoidable (and often undetected as well) imperfections (physical and/or, geometrical) which cannot be fully taken into account during theoretical calculations. In addition to the inherent imperfections, if the material of the structure itself shows exceptional behaviors (for instance, occurrence of phase change under load at room temperature) it is justified to determine the buckling load of a structure directly from the experimental data.

It was found from the present study that quite astonishingly too short superelastic SMA columns do not fail due to buckling simply after the first peak load is reached or the mode of deformation is changed. Those columns fail only after exceptionally large deformation takes place beyond the first point of instability. Thus, both the prebuckling and the postbuckling zones of the deformed columns have been determined for the complete cycles through the axial load versus end shortening (P–Δ) curves or, mathematically through the equilibrium paths. As a result, in this study, the buckling loads are determined accurately in a realistic way. Moreover, some interesting postbuckling behaviors, particularly those of the SMA columns, are also observed from the P–Δ curves for a complete cycle.

2. Test conditions and experimental method

The materials, configurations and conditions used in this experiment are as follows. Column materials: SMA (Ti49.3 at.% Ni50.2 at.% V0.5 at.%), stainless steel (SUS304), and aluminum. Diameter = 2 mm, L (mm) = 14, 19, 24, 34, 44, 54, 64, 74, 84, 109, 134, 159, 184. Room temperature range = 23–30 °C. $A_f = -3$ °C. Machine used: Instron. Speed of the cross-head during loading–unloading cycle = 2 mm/min.

At first, the columns (solid rods of 2 mm diameter) were inserted into the holes of the loading fixtures (Fig. 1). One of the fixtures was fixed while the other was attached to the movable cross-head of the Instron machine. As the test started, the axial deformation (more precisely, the end shortening) of the column due to the load P was directly measured by δ, the linear displacement of the moving fixture. During compressive loading on the column, the moving fixture moved towards the fixed one until its predetermined final position was reached. In the mean time, the column buckled and had enormous deformations. Immediately after the final point of displacement was reached, the moving fixture was moved away from the fixed one. Thus, the largely deformed column was allowed to gradually recover its shape. The unloading process was stopped and the cycle ended when P became approximately zero.

The P–Δ curves during a complete cycle are necessary to determine the buckling loads and also to observe different postbuckling behaviors of the columns. It should be mentioned here that, for columns with $L/k = 28$ and 38, the unloading process started when the values of Δ (that is, δ/L) were 10% and 5.5%, respectively. These large deformations were necessary to observe the interesting P–Δ curves of the short SMA columns. All other columns were unloaded from $\Delta = 3\%$. The value of Δ measured after the complete cycle corresponds to the residual axial strain (ε), that gives an evaluation of the capability of shape recovery of the columns made of different materials.

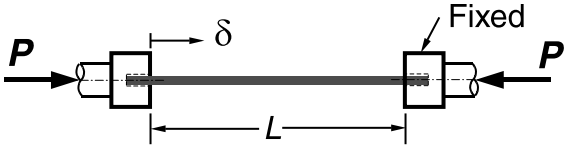

Fig. 1. Column inserted into the loading fixtures.

3. Results and discussions

To precisely observe the buckling and postbuckling behaviors of a column, the corresponding P–Δ curve was obtained much beyond the point of instability. Before discussing and interpreting those P–Δ curves, the material properties of the superelastic SMA, that is, its stress–strain curves in tension and compression and the SIMT should be discussed first.

For simplicity, the idealized stress–strain diagram (for $T > A_f$), that actually resembles the hysteresis of tensile test for the superelastic SMA is depicted in Fig. 2(a). The first linear portion of Fig. 2(a) represents the parent austenite phase. During loading, transformation of the SIM phase starts at the critical stress. After the SIMT (marked by low material stiffness), SMA is in the fully martensite phase. When unloaded, the SMA returns to its parent austenite phase and recovers the strains through a hysteresis, which is known as the pseudoelasticity or SE (Fig. 2(a)). The nominal stress–strain curves for the materials obtained from the experimental data are presented in Fig. 2(b). The tensile test data shows that, the SMA material exhibits pretty high stiffness (although there is plastic slip) if loading continues after complete SIMT. It is noteworthy

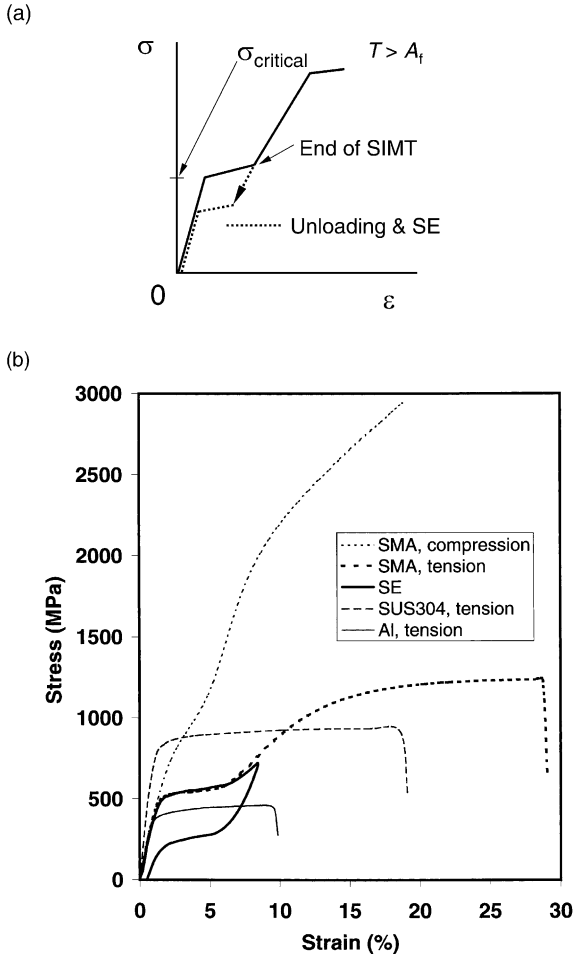

Fig. 2. (a) Idealized stress–strain curve for the superelastic SMA. (b) Nominal stress–strain curves for the superelastic SMA, SUS304 and Al rods (the deformation of the specimen was measured directly from the cross-head displacement of the Instron machine).

from the tensile tests that the Al rod has the lowest yield strength, while for large strains after the SIMT the SMA rod can carry the highest load.

Unlike the superelastic SMA, both Al and SUS304 exhibit more or less the similar nature of stress–strain curves in compression and tension. On the other hand, it is a well-known fact that the behaviors of the Nitinol SMA in tension and compression are very much different particularly for SE (Auricchio and Sacco, 1997; Orgeas and Favier, 1995). The experimental results from the present study also verifies that the compressive strength of the superelastic SMA is significantly higher than its tensile strength, particularly for large strains (Fig. 2(b)). Unlike the tensile stress–strain curve there is no distinct plateau for a particular range of strains and as such the start and finish of the SIMT process is rather difficult to locate for the compressive stress–strain curve. It appears that for the compression test the SIMT process is indicated by a slight change in slope of the stress–strain curve (Fig. 2(b)). It should be noted here that different specimens were used for tension and compression tests under the same test conditions as already mentioned. Following Johnson (1972), to avoid any chance of buckling of the specimen during the pure compression test, L/k was kept less than 12.

The comparative buckling and postbuckling behaviors of the columns with different L/k are demonstrated by the axial compressive load (P) versus the end shortening (Δ) curves as shown in Fig. 3(a)–(f). It can be observed that the nature of the P–Δ curves for the SMA columns changes quite notably with L/k. For the shortest SMA column (i.e., with $L/k = 28$) the load increases after a distinct change in the mode of deformation (Fig. 3(a)). It should be noted that the term 'change in the mode of deformation' is used here to refer to the distinct change in the slope of the P–Δ curve for a column. The portion of the P–Δ curve connecting the two modes of deformation contains a point of instability for all the columns. Ideally, the first and the second modes of deformation should correspond, respectively, to the initial straight shape and the buckled shape of the columns. But, in fact, owing to the unavoidable initial imperfections, the column is slightly bent (may not be identified easily) during the first mode of deformation. While, the second mode of deformation corresponds to the markedly bent configuration of the column after it passes through the point of instability. As seen, unlike the Al and SUS304 columns, quite remarkably, this SMA column can sustain significantly high load during its secondary mode of deformation (Fig. 3(a)). On the other hand, for $L/k = 38$, the P–Δ curve of the SMA column (Fig. 3(b)) shows a valley between two distinct peak loads (the second peak being slightly higher than the first one). The above characteristic is contrary to the general trend that load falls off monotonously for any further compression after the first distinct peak load (which is also a point of instability) on the equilibrium configuration path (P–Δ curve) of a column.

By numerical simulation, Auricchio and Sacco (1997) demonstrated that for pure bending of a Nitinol SMA beam, with different properties in tension and compression, the axial strain has a non-monotonous response with the bending moment during loading and unloading. The complicated movement of the neutral axis of the cross-section of the beam due to SIMT leads to such peculiar response. Obviously, the instability of a column and pure bending of a beam are very different phenomena. However, it appears that for the present study too, the occurrence of SIMT along with the phenomenon of buckling may cause the load to change non-monotonically with deformation for the superelastic SMA columns. Thus the unique buckling and postbuckling behaviors of the short superelastic SMA columns are qualitatively explained in the following paragraphs.

The pure compression stress–strain curve (Fig. 2(b)) will dominate the buckling and postbuckling behaviors particularly for too short superelastic SMA columns ($L/k = 28$) as shown by Fig. 3(a). Obviously for this column, at one stage of the prebuckling compression, the SIMT is initiated within the column material. As discussed, unlike the tensile stress–strain curve, there is no distinct plateau during the SIMT process for the compressive stress–strain curve. Rather the initiation of the SIMT may be marked by a slight and smooth decrease in the material stiffness (Fig. 2(b)). Highly compressed SMA column (which is prone to buckling if there is any kind of disturbance) gradually approaches the first point of instability as its load–deformation curve corresponds to the initiation of the SIMT, that is, slight decrease in stiffness of the

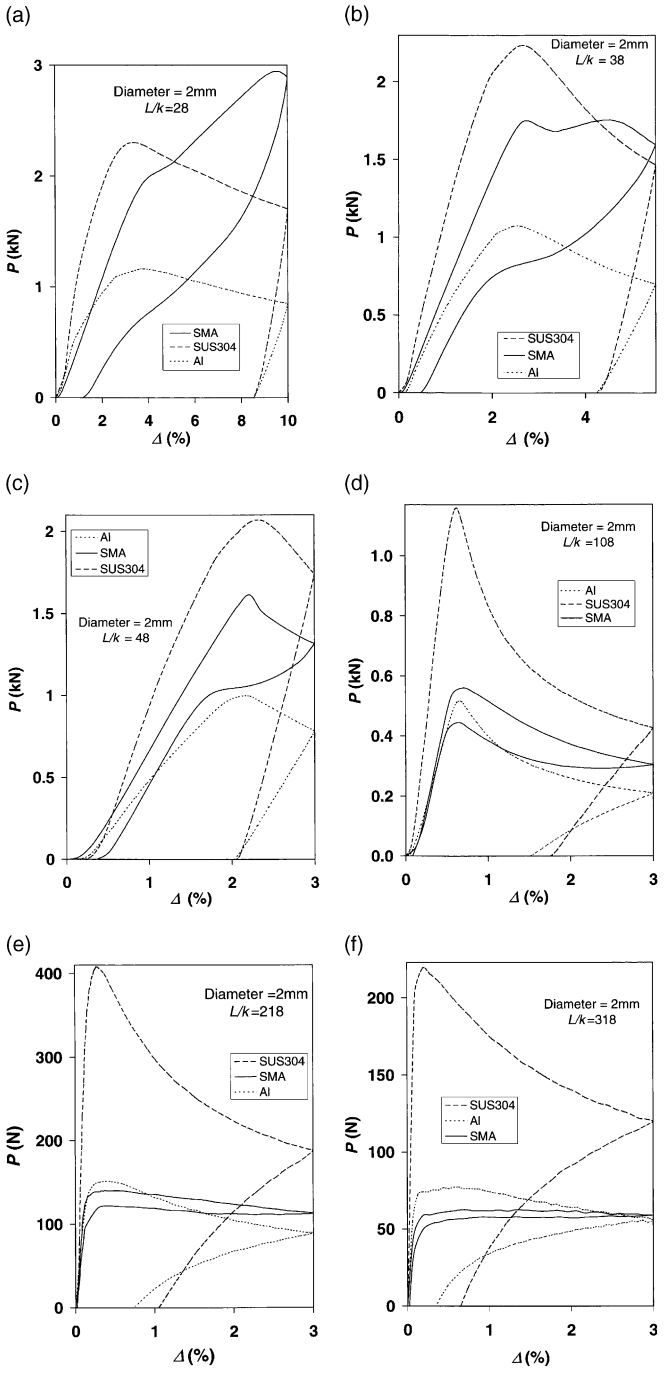

Fig. 3. Comparative load-end shortening curves during a cycle for the SMA, SUS304, and Al columns with L/k corresponding to (a) 28, (b) 38, (c) 48, (d) 108, (e) 218 and (f) 318.

compressive stress–strain curve. The bending effect causes the innermost fibers of the cross-section of the column to be under higher compressive strains compared to the outermost fibers. Thus the innermost fibers

first complete the SIMT. After the SIMT is completed, the material stiffness is significantly high particularly for the compressive stress–strain curve (Fig. 2(b)). Thus because of its peculiar material property, quite unusually, after the first point of instability, this column can assume highly stable postbuckling configuration. During the secondary mode of deformation, the bending effect is resisted by the increasing material stiffness that enables this column to carry high load until the second point of instability is appeared. Numerical simulation of the buckling and postbuckling behaviors of the short superelastic SMA columns (based on compressive stress–strain curve), which is being carried out, has verified the above facts. The P–Δ curve of Fig. 3(a) indicates that after pretty large deformation ($\delta/L = 9.6\%$) this column ultimately fails at the second point of instability at a load much higher than that for SUS304 column.

Now let us discuss the P–Δ curve with two peaks for the SMA column with $L/k = 38$. The compressive stress–strain curve will also dominate the behavior of this column though it has less bending stiffness compared to that with $L/k = 28$. Significantly high stress prior to the first peak (when Δ is about 2.7% in the P–Δ curve of Fig. 3(b)) can easily initiate the SIMT within the column material. After the first peak (which is a point of instability for the column) is reached, the load falls off to a valley and the column is further deformed. It can be verified that, compared to the primary mode of deformation prior to the first peak, large deformation takes place with small change in load between the first peak and the valley of the P–Δ curve (Fig. 3(b)). Thus, as the load slowly falls from the first peak to the valley, each strained cross-section of the column is added with rapidly increasing strains. Due to the bending strains, for all the critically strained cross-sections of the column, the fibers that are farthest from the neutral axis, first undergo complete phase transformation. The material stiffness starts increasing as fibers gradually complete SIMT. Consequently, the bending effect due to the load P, is overcome by the increasing resisting moment due to significant increase in the material stiffness. Thus, the load again increases slowly from the valley until buckling occurs at the second peak (Fig. 3(b)). Obviously, the increase in the material stiffness after SIMT can more significantly contribute to resist the buckling of the SMA columns having lower L/k. Thus, the SMA column with $L/k = 28$ shows much more buckling resistance compared to that with $L/k = 38$ after the first point of instability.

The reasons for the short SMA columns' unique buckling resistance are explained here qualitatively. It is also noteworthy that the prebuckling stiffness of the SUS304 column is higher than that of the SMA column. Therefore, it can be concluded from the present study that the special nature of the stress–strain curves in tension and compression along with the SIMT itself enable the short SMA columns to exhibit the above discussed exceptional behaviors.

Let us next discuss the variation of the buckling loads with L/k for different materials. The buckling loads for the columns (as shown in Table 1 and Fig. 4) are determined from the peak loads (after which the load falls off monotonously) of the P–Δ curves of Fig. 3(a)–(f). Naturally, shorter is the column, higher is its buckling load and larger is the corresponding prebuckling deformation (Fig. 3(a)–(c)). For a certain value of the axial load, the most critical section of the column becomes fully plastic and initiates its failure. As verified by experiments, Al has the lowest yield strength among the three materials. Thus Al columns with $L/k = 28$–108, have the lowest buckling loads. Moreover, once started, plastic deformation continues without appreciable change in the load's magnitude until fracture occurs for the case of Al and SUS304 rods (Fig. 2(b)). That is why the buckling loads change by small magnitude with L/k if the SUS304 and Al columns are too short as shown by Fig. 4 and Table 1. On the other hand, among the three materials, SMA column's buckling load increases most significantly with the decreasing L/k, and ultimately, it exceeds the buckling load of the SUS304 column (Table 1 and Fig. 4). As already discussed, for too short columns SIMT is triggered on during continuous compression. After the complete SIM transformation the stiffness of the SMA materials increases significantly and for large strains the compressive strength is much higher than its tensile strength. This increase of the material stiffness after the SIMT helps too short SMA columns to easily sustain higher buckling loads compared to SUS304 columns. However, unlike the too short SMA columns, the slender ones cannot sustain much axial compression and buckle elastically while they are in

Table 1
Buckling loads (P_{cr}) and residual axial strains (ε) of the columns[a]

L/k	Material	P_{cr} (N)	ε (%)	L/k	Material	P_{cr} (N)	ε (%)
28	SUS304	2305, 2325, 2374	8.5	148	SUS304	765, 769, 769	1.5
	SMA	2930, 2943, 2972	1.2		SMA	280, 285, 286	0.15
	Al	1163, 1163, 1170	8.5		Al	299, 301, 301	1.2
38	SUS304	2235, 2241, 2261	5.6	168	SUS304	638, 648, 648	1.4
	SMA	1756, 1776, 1805	0.9		SMA	226, 232, 234	0.15
	Al	1071, 1072, 1100	5.6		Al	240, 245, 254	1.0
48	SUS304	2041, 2060, 2070	2.0	218	SUS304	426, 427, 427	1.1
	SMA	1481, 1501, 1614	0.35		SMA	137, 139, 143	0.04
	Al	981, 991, 991	2.0		Al	153, 154, 155	0.75
68	SUS304	1638, 1717, 1815	2.0	268	SUS304	294, 295, 307	0.9
	SMA	1020, 1060, 1079	0.3		SMA	90, 91, 91	0.04
	Al	814, 824, 834	1.9		Al	103, 105, 105	0.5
88	SUS304	1364, 1373, 1373	1.9	318	SUS304	217, 217, 218	0.65
	SMA	697, 716, 726	0.2		SMA	65, 66, 66	0.02
	Al	638, 667, 667	1.7		Al	71, 74, 76	0.35
108	SUS304	1118, 1158, 1177	1.8	368	SUS304	165, 167, 167	0.55
	SMA	520, 540, 559	0.2		SMA	52, 53, 53	0.02
	Al	500, 520, 520	1.5		Al	53, 56, 59	0.22
128	SUS304	893, 922, 932	1.6				
	SMA	358, 363, 367	0.2				
	Al	378, 383, 387	1.3				

[a] For each type of material at least three tests were performed for a particular L/k. The highest P_{cr} and the corresponding maximum ε are shown. P_{cr} for SMA column with $L/k = 38$ corresponds to the second peak of the P–Δ curve.

the austenite phase. Thus, having the lowest Young's modulus among the three materials, too slender SMA columns have the lowest buckling loads. Table 1 shows that for $L/k = 128$–368, the buckling loads of Al columns are higher than those of SMA columns by 5–15% (see also Fig. 3(e) and (f)). Usually this difference increases with the increasing slenderness ratios. In the same manner, for the above range of the slenderness ratio the buckling loads for SUS304 columns are much higher (about 2.5–3.3 times) than those for SMA columns.

Since the buckling loads of the columns are highly imperfection sensitive, it is essential to check the accuracy of the present experimental results by theory. The easiest way to check the accuracy of the experimental buckling loads of Table 1, is to make use of the famous Euler formula ($4\pi^2 EI/L^2$, symbols having their usual meanings) for both ends-clamped slender columns. As shown in Table 1, for the columns made of stainless steel (SUS304) with $L/k = 218$, 268, 318 and 368, the highest buckling loads are 427, 307, 218 and 167 N, respectively. The Young's modulus (E) of SUS304 is around 200 GPa. Accordingly, the corresponding Euler buckling loads are 522, 345.4, 245.3 and 183.2 N, respectively. Euler formula, based on eigenvalue solutions is for ideal conditions and thus predicts higher buckling loads for columns. Even then the experimental buckling loads are found to be 82–91% of their theoretical values according to the above formula. Higher is the slenderness ratio, better is the prediction by theory. Since the prebuckling stress for a particular column material exceeds the proportional limit below certain slenderness ratio, the above formula cannot be used in those cases to predict the buckling loads. However, good agreement between the theoretical and the experimental buckling loads for slender columns proves that the present experimental method is an easy and realistic way to find out the buckling loads for columns. Thus it can be concluded

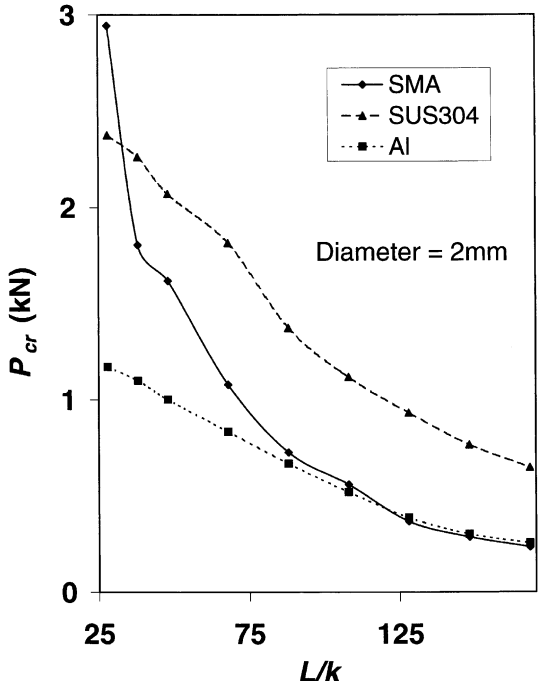

Fig. 4. Buckling load versus slenderness ratio (28–168) for the superelastic SMA, SUS304, and Al columns.

that the results obtained for columns of other materials and of different slenderness ratios using the same method are also accurate.

One noteworthy postbuckling characteristic of the superelastic SMA columns (if not too short) is that, having too small values of residual strain (ε) after a complete cycle, they are able to exhibit almost the same pattern of P–Δ curves for a few repeated loading–unloading cycles. The above excellent capability is attributed to SMA's superelasticy. Huge postbuckling compression on the columns initiates SIMT that is again converted to pure austenite phase upon unloading allowing the columns to recover large strains. The measured values of ε after the complete cycle (Table 1) give a rough estimation of the shape recovery capability of the buckled columns. As seen, higher is the L/k, better is the shape recovery. For $L/k = 88$–168, ε is within 0.2% and for too slender SMA columns ($L/k = 218$–368), it is negligibly small (within 0.04%). Thus it can be concluded that those SMA columns ($L/k = 88$–368) will show more or less the similar unique buckling and postbuckling behaviors (as shown by Fig. 3(d)–(f)) for a few cycles. However, shorter SMA columns ($L/k = 28$–68) partially recover the initial shapes after complete unloading. Consequently, the buckling loads start falling gradually if the cycles are repeated more than twice (Fig. 5). On the other hand, both the Al and SUS304 columns suffer large permanent deformation in all the cases as seen from Fig. 3(a)–(f) and Table 1, and therefore found to be plastically bent when completely unloaded. Among the three materials, ε increases most significantly for Al columns with the decreasing L/k, although, slender Al columns show small ε. It is noteworthy that for the SMA columns with $L/k = 68$, the cumulative residual strain even after three consecutive cycles is much smaller than those of the Al and SUS304 columns after the first cycle (Fig. 5 and Table 1). Moreover, as seen, the SMA column with $L/k = 28$ can sustain much higher load and deformation before failure than those of a SUS304 column. Thus short superelastic SMA columns can be good candidates as structural elements in practical applications where high load carrying capability is required for a few repeated loading–unloading cycles.

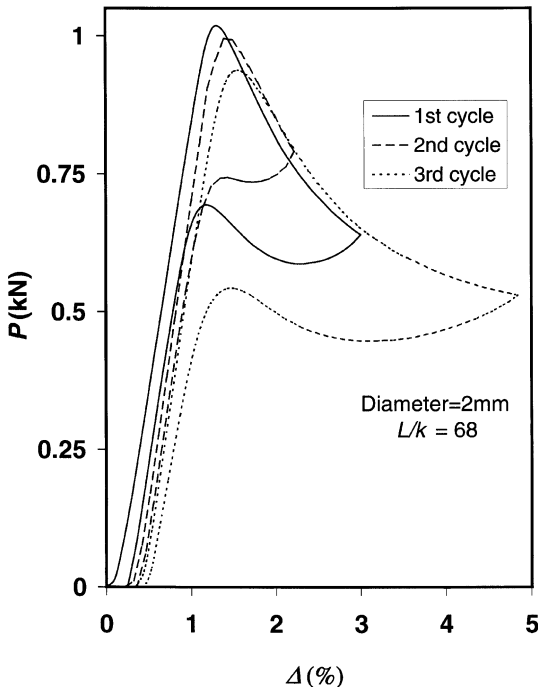

Fig. 5. Load-end shortening curves for three consecutive cycles for the SMA column with $L/k = 68$.

Table 2
Percent fall between the load at the point of instability and load at $\Delta = 3\%$

L/k	368	318	268	218	168	128	88
SMA	4	5	12	20	27	36	43
Al	20	26	31	44	51	57	58
SUS304	38	45	49	55	63	63	58

Table 2 shows a comparison of load sustaining capability of the columns in the postbuckling region. Although the SMA column with $L/k = 38$ exhibits some exceptional behaviors, it is found that load falls off monotonously for the case of other columns if the compression is continued beyond the first peak on the P–Δ curves up to the final point of loading. As seen from Table 2, among the three materials, the load falls off most drastically for the SUS304 column during the postbuckling compression. It can be also verified that shorter is the column, more notably the load falls off. However, compared to the Al and SUS304 columns, the superelastic SMA columns, particularly the slender ones, can easily sustain the load with the least change in magnitude after buckling (Fig. 3(e) and (f)). For instance, for SMA columns with $L/k = 368$, the load falls off from its peak value (that is, from the buckling load) only by 4% in magnitude up to the last point of loading. For the same L/k, the fall in load's magnitude is five times more for Al columns and almost 10 times more for SUS304 columns (Table 2).

Next, let us discuss another remarkable phenomenon exhibited by some of the SMA columns during the unloading process. The shape recovery process of the buckled columns actually starts with the unloading

and ends when the load becomes approximately zero. It is found that for the slenderness ratio of 68–128, the recovery force of the SMA columns increases quite significantly, as if the pronouncedly deformed SMA columns push the loading fixtures during the unloading period (Figs. 3(d) and 5). The above phenomenon is quite contrary to the general notion that load falls off monotonously during unloading of a buckled column. However, for slender SMA columns ($L/k = 218$–368), the recovery force does not change much during the unloading process, and starts falling linearly after closely approaching the initial portion of the loading curve (Fig. 3(e) and (f)).

It seems that for a particular L/k whether the recovery force of the SMA column will increase notably or not, depends on the nature of its P–Δ curve (equilibrium path) during loading. As noted, after buckling slender SMA columns ($L/k = 218$–368) can sustain the load with least changes in magnitude up to the last point of loading. During unloading of these slender columns the recovery force does not change much. On the other hand, the recovery force increases significantly for the SMA columns with $L/k = 68$–128. It is noted that, for these particular SMA columns (that is, with $L/k = 68$–128), load falls off much more compared to the slender columns ($L/k = 218$–368) if the compression is continued up to $\Delta = 3\%$ or more (Table 2 and Figs. 3(d) and 5). Although the load falls off significantly during the postbuckling deformation, due to its SE, the buckled SMA column is still capable of recovering the initial shape upon unloading. As a result, at one stage during the shape recovery process the bent column starts pushing the fixture until the rest of the shape is almost recovered. Thus the P–Δ curve during unloading (shape recovery) process gradually increases to a maximum load. The shape is almost recovered at the maximum point and the recovery force does not increase any more with further displacement of the fixture. The remaining amount of strain is recovered linearly resembling an elastic unloading curve.

Finally, the effect of room temperature change on the unique buckling and postbuckling behaviors of the superelastic SMA columns should be clarified. As mentioned, for the present study the room temperature was always much higher than the austenite finish temperature of the SMA, leading to its property of SE during unloading. As a result, SMA columns, particularly the slender ones can recover their shapes with small residual strains even after too large postbuckling deformations (Fig. 3(e) and (f)).

From the results of pure tension tests it is a well-known fact that, the critical stress necessary to induce SIMT process may increase notably and the stress–strain hysteresis change with significant increase in temperature (of course, the temperature should not be so high to soften the material) for the superelastic SMA (Otsuka and Wayman, 1998; Liang and Rogers, 1997; Gandhi et al., 1998). Thus, if both the tensile and compressive properties of the materials change notably with changing temperatures, it is likely to affect the buckling behaviors of the columns. A comprehensive study concerning the above point will be separately carried out in near future. However, for the present case, many tests were performed for a long span of time during which the room temperature was within 23–30 °C. Practically, any change in the mechanical properties of the materials, due to such a small temperature variation may be treated as insignificant. As discussed slender SMA columns buckle elastically in the austenite phase while the short ones buckle plastically after SIMT. That the buckling and postbuckling behaviors of the shortest ($L/k = 28$) superelastic SMA columns (three different specimens) are very similar for small temperature variation may be clarified from Fig. 6. As seen, the P–Δ curves during the whole cycles are almost identical for room temperatures 23 and 26 °C. Though for the room temperature of 25 °C, the P–Δ curve shows slight deviations, it can be treated as negligible as the variation in the buckling load is within 1%. Since the slight variation in room temperature has negligible effect on the buckling and postbuckling behaviors of the shortest SMA column, it can be concluded that for the present study, it (the temperature effect) would be also negligible for the case of all other columns particularly the slender ones (which buckle elastically and before the SIMT). Moreover, buckling behaviors of columns are highly imperfection sensitive. Thus the effect of geometrical or, physical imperfections may be more important than the effect of slight temperature change.

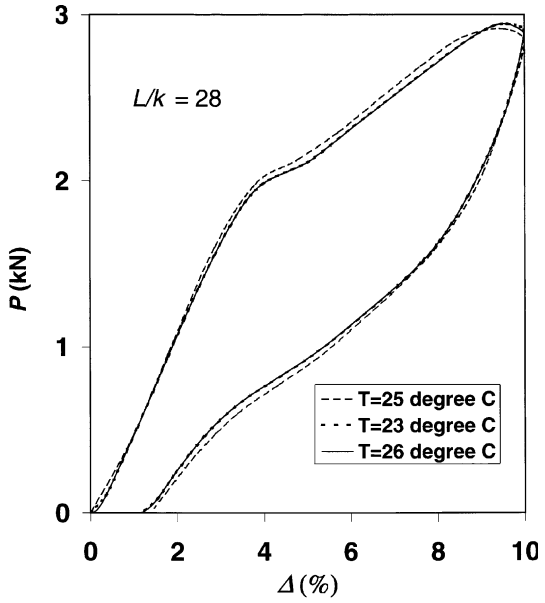

Fig. 6. Load-end shortening curves for three different room temperature for the SMA column with $L/k = 28$.

4. Conclusions

Using a loading–unloading cycle, some interesting and useful buckling and postbuckling characteristics of the superelastic SMA columns were observed from the present study. Those phenomena depend largely on the slenderness ratio (L/k). For example, the P–Δ curves for the short SMA column with $L/k = 38$ shows two distinct peak loads during loading, the second one being the higher, quite contrary to the general trend that load falls off monotonously for other columns during any further compression beyond the first peak load. Similarly, for $L/k = 28$, the SMA column can sustain significantly high load (even higher than that of a SUS304 column) after a distinct change in the mode of deformation. It is found that, too slender SMA column has the lowest buckling loads among the three materials used in the investigation. Because of high material stiffness after the SIMT, the buckling load of the superelastic SMA columns increases most significantly for decreasing L/k, and ultimately exceeds that of the SUS304 column.

It is also observed that the SMA columns, if not too short, can sustain the buckling load with least change in magnitude if the compression is continued much beyond the point of instability. Moreover, during unloading from the postbuckling state, the recovery force of the SMA columns (for $L/k = 68$–128) increases significantly, another remarkable phenomenon, quite contrary to the general conclusions that load falls off monotonously during unloading of a buckled column. Furthermore, if the slenderness ratio is not too low, the initial shape before the deformation is recovered with small residual strains when the profusely deformed SMA columns are unloaded from the postbuckled state. Thus they can be used for repeated cycles to show the similar buckling and postbuckling behaviors.

The above discussed unique phenomena can be attributed to the special nature of SMA's stress–strain curve and the SE itself. On the other hand, for the whole range of slenderness ratio considered in this study, Al and SUS304 columns show large residual strains after the complete cycle.

References

Auricchio, F., Sacco, E., 1997. A superelastic shape-memory-alloy beam model. Journal of Intelligent Material Systems and Structures 8, 489–513.

Brinson, L.C., 1993. One-dimensional constitutive behavior of shape memory alloys: thermomechanical derivation with non-constant material functions and redefined martensite internal variable. Journal of Intelligent Material Systems and Structures 4, 229–242.

Gandhi, F., Wolons, D., Malovrh, B., 1998. Experimental investigation of the pseudoelastic hysteresis damping characteristics of shape memory alloy wires. Journal of Intelligent Material Systems and Structures 9, 116–126.

Johnson, W., 1972. Impact Strength of Materials. Edward Arnold, London.

Kamita, T., Matsuzaki, Y., 1998. One dimensional pseudoelastic theory of shape memory alloys. Smart Materials and Structures 7, 489–495.

Liang, C., Rogers, C.A., 1997. Design of shape memory alloy springs with applications in vibration control. Journal of Intelligent Material Systems and Structures 8, 314–322.

Orgeas, L., Favier, D., 1995. Non-symmetric tension-compression behaviour of NiTi alloy. Jornal de Physique IV, Colloque (France) 5 (c8, pt.2), 605–610.

Otsuka, K., Wayman, C.M., 1998. Shape Memory Materials. Cambridge University Press, Cambridge, MA.

Tobushi, H., Okumura, K., Endo, M., Takata, K., 2000. Stress-induced martensite transformation behavior and lateral strain of TiNi shape memory alloy. Proceedings of the 11th ICAST. Nagoya, Japan, pp. 367–374.

Thompson, J.M.T., Hunt, G.W., 1973. A General Theory of Elastic Stability. Wiley, UK.